

1       **Potential of 5-fluorouracil encapsulated in zeolites as drug**  
2       **delivery systems for *in vitro* models of colorectal carcinoma**

3  
4       Natália Vilaça,<sup>a</sup> Ricardo Amorim,<sup>b,c</sup> Ana F. Machado,<sup>a</sup> Pier Parpot,<sup>a</sup> Manuel F.R. Pereira,<sup>d</sup>  
5       Mariana Sardo,<sup>e</sup> João Rocha,<sup>e</sup> António M. Fonseca,<sup>a</sup> Isabel C. Neves\*<sup>a</sup> and Fátima Baltazar\*<sup>b,c</sup>

6  
7  
8       <sup>a</sup>*Centre of Chemistry, Chemistry Department, University of Minho, Campus de Gualtar,*  
9       *4710-057 Braga, Portugal - E-mail: (ineves@quimica.uminho.pt)*

10      <sup>b</sup>*Life and Health Sciences Research Institute (ICVS), School of Health Sciences, University of*  
11      *Minho, Campus Gualtar, Braga, Portugal - E-mail: (fbaltazar@ecsaude.uminho.pt)*

12      <sup>c</sup>*ICVS/3B's - PT Government Associate Laboratory, Braga/Guimarães, Portugal*

13      <sup>d</sup>*Laboratory of Catalysis and Materials (LCM), Associate Laboratory LSRE/LCM, Faculdade*  
14      *de Engenharia, Universidade do Porto, Rua Dr. Roberto Frias, 4200-465 Porto, Portugal*

15      <sup>e</sup>*CICECO – Chemistry Department, University of Aveiro, Campus de Santiago, 3810-193*  
16      *Aveiro, Portugal*

17  
18  
19      **ABSTRACT**

20      The studies of potentiation of 5-fluorouracil (5-FU), a traditional drug used in the treatment of  
21      several cancers, including colorectal (CRC), were carried out with zeolites Faujasite in the  
22      sodium form, with different particle sizes (NaY, 700 nm and nanoNaY, 150 nm) and Linde  
23      type L in the potassium form (LTL) with a particle size of 80 nm. 5-FU was loaded into  
24      zeolites by liquid-phase adsorption. Characterization by spectroscopic techniques (FTIR, <sup>1</sup>H  
25      NMR and <sup>13</sup>C and <sup>27</sup>Al solid-state MAS NMR), chemical analysis, thermal analysis (TGA),  
26      nitrogen adsorption isotherms and scanning electron microscopy (SEM), demonstrated the

27 successful loading of 5-FU into the zeolite hosts. *In vitro* drug release studies (PBS buffer pH  
28 7.4, 37 °C) revealed the release of 80-90% of 5-FU in the first 10 min. To ascertain the drug  
29 release kinetics, the release profiles were fitted to zero-order, first-order, Higuchi, Hixson-  
30 Crowell, Korsmeyer-Peppas and Weibull kinetic models. The *in vitro* dissolution from the  
31 drug delivery systems (DDS) was explained by the Weibull model. The DDS efficacy was  
32 evaluated using two human colorectal carcinoma cell lines, HCT-15 and RKO. Unloaded  
33 zeolites presented no toxicity to both cancer cells, while all DDS allowed an important  
34 potentiation of the 5-FU effect on the cell viability. Immunofluorescence studies provided  
35 evidence for zeolite-cell internalization.

36

37 **Keywords:** Zeolites; 5-fluorouracil (5-FU); encapsulation; drug delivery; cytotoxicity;  
38 potentiation

39

## 40 **1. Introduction**

41 Colorectal carcinoma (CRC) is one of the most common types of cancer in industrialized  
42 countries, slightly more prevalent in men than women [1]. Generally, the treatment of CRC  
43 includes surgery, radiotherapy and/or chemotherapy. The treatment design depends, however,  
44 largely on the cancer stage. Although for patients with an early-stage disease, surgery gives a  
45 relatively good prognosis; patients in a more advanced disease stage often require adjuvant  
46 chemotherapy to reduce cancer and the high risk of recurrence [2-4].

47 5-Fluorouracil (5-FU) has been in use for about 50 years [5], being one of the most effective  
48 chemotherapeutic agents in the treatment of CRC, stomach, breast, and head & neck cancers  
49 [6,7]. Despite the progress made with the introduction of new cytotoxic agents and medical  
50 practices, the survival rates of CRC patients changed little over the past 20 years [8-12],  
51 justifying the need for more effective therapies.

52 Therapy with classical drugs such as 5-FU, has important toxic side effects. Thus,  
53 encapsulation in sustained delivery systems may contribute to reduce these side effects and  
54 maybe allow oral administration. 5-FU is administered intravenously due to its variable  
55 gastrointestinal absorption and rapid degradation [13,14]. There are several advantages to oral  
56 drug administration, including patient's convenience and the reduced costs associated with  
57 drug preparation and administration [4]. The efficacy of 5-FU therapy may also be enhanced  
58 and its toxicity diminished by association with delivery systems that selectively convey this  
59 active agent while, at the same time, reduce its toxicity [15]. Moreover, encapsulation may  
60 allow drugs to be released in a controlled way to the cancer area, preventing degradation of  
61 the anticancer drug [4,15,16].

62 Several recent studies showed that the potential of zeolites in medical applications is due to  
63 their structural properties and stability in biological environments [17,18]. Zeolites have also  
64 been explored as suitable hosts for the encapsulation of drug molecules, in search for efficient  
65 DDS. Both zeolites and drugs have been administrated simultaneously to a patient without  
66 loss of the individual pharmacological effect of the drugs [17-28].

67 Zeolites are solid hydrated crystalline materials with frameworks comprising silicon,  
68 aluminum and oxygen and featuring nano-channels and cages of regular dimensions [29]. The  
69 pores of zeolites are open to the surrounding medium, thus allowing diffusion of molecules  
70 from the exterior to the interior of the zeolite particle. Zeolites exhibit a large specific surface  
71 area, typically in excess of  $400 \text{ m}^2 \text{ g}^{-1}$ , with most of this area being internal (void volume  
72 above  $0.10 \text{ cm}^3 \text{ g}^{-1}$ ), and are very stable in different media [29]. The water molecules within  
73 the cavities are loosely bound and are easily removed upon heating, resulting in a high surface  
74 area and accessible pore volume [29].

75 In previous studies we have reported the preparation of DDS based on zeolite structures with  
76 the experimental anticancer drug  $\alpha$ -cyano-4-hydroxycinnamic acid (CHC) and demonstrated  
77 its efficacy against colorectal carcinoma cells [30,31]. As a continuation of this line of

78 research, the anticancer drug 5-FU was encapsulated into two zeolites with diverse  
79 frameworks and particle size. Zeolite L is an aluminosilicate bearing parallel one-dimensional  
80 channels with pore openings of *ca.* 0.71 nm in diameter, able to host a large variety of small  
81 molecules [32]. Zeolite Y consists of supercages with a diameter of 1.18 nm, sharing a 12-  
82 membered ring with an aperture of 0.74 nm [33], suitable to accommodate various  
83 compounds [33-36]. These new DDS were characterized by a range of methods, spectroscopic  
84 techniques (FTIR and <sup>13</sup>C and <sup>27</sup>Al solid-state MAS NMR), scanning electron microscopy  
85 (SEM), thermogravimetric analysis (TGA), nitrogen adsorption isotherms and elemental  
86 analysis. The effect of zeolites and DDS was evaluated on HCT-15 and RKO human colon  
87 carcinoma cell viability. Zeolite-cell internalization was also assessed.

88

## 89 **2. Materials and Methods**

### 90 **2.1. Materials**

91 Linde Type L zeolite powder in the potassium form (NanoZeolite LTL, Si/Al = 3.40) with ~  
92 80 nm average particle size was purchased from NanoScape. Two faujasite zeolites with  
93 different particle sizes were commercially available in the sodium form and as a powder; NaY  
94 zeolite (Si/Al = 2.83, CBV100) was obtained from Zeolyst International and nanoNaY zeolite  
95 (NanoFAU-Y, Si/Al = 2.25) from NanoScape. 5-fluoro-1H-pyrimidine-2,4-dione usually  
96 know as 5-fluorouracil (5-FU) was used as obtained from Sigma-Aldrich (99%). Rhodamine  
97 B was supplied by Merck ( $\geq 90\%$ ).

### 98 **2.2. Preparation of 5-FU@zeolites**

99 Loading of 5-FU into zeolites was based on a previously established procedure [30,31].  
100 Before 5-FU loading, the zeolite powders were dehydrated at 120 °C overnight in order to  
101 remove the water from the pores. 5-FU loading into the zeolites was achieved by mixing 100  
102 mg of each zeolite with a solution of 5-FU (130 mg, 0.99 mmol) in acetone (15 mL) as a  
103 solvent and was stirred (300 rpm) for 48 h at room temperature. The mixture was filtered and

104 the resulting DDS dried in an oven at 60 °C for 12 h. This temperature is enough to evaporate  
105 the acetone solvent. Throughout the manuscript, the obtained DDS will be referred to as 5-  
106 FU@zeolite, where zeolite represents the structure of the zeolite used. Also, preliminary  
107 studies with other solvents in which 5-FU is soluble (ethanol and methanol) were carried out  
108 under the same experimental conditions to which the 5-FU@zeolite samples were submitted.  
109 After preparation of the DDS, these solvents remained adsorbed in the zeolite structures and  
110 are toxic to the cell lines studied. The amount of loaded 5-FU was measured using  
111 thermogravimetric analysis (TGA). In order to evaluate the solvent effect, the zeolites were  
112 prepared with 15 mL of solvent, using the same experimental conditions as the DDS samples.  
113 The cellular location of NaY was monitored by loading this zeolite with Rhodamine B. This  
114 compound was loaded into NaY by stirring (300 rpm, 48h at room temperature) a mixture of  
115 100 mg of zeolite in a solution of Rhodamine B (20 mg, 0.042 mmoles) in acetone (15 mL).  
116 The reaction vessel was lined with foil to protect from light. The mixture was filtered and the  
117 obtained solid (referred to as RB@NaY) was dried at 60 °C for 12 h.

### 118 ***2.3. Drug release studies of 5-FU@zeolites***

119 Drug release from loaded 5-FU@zeolite samples was studied by HPLC analysis at  $\lambda = 260$   
120 nm. The simulated body fluid was made using known amounts of a buffer solution of sodium  
121 monobasic phosphate and sodium dibasic phosphate (PBS). Known amounts of the DDS were  
122 mixed (10 mg) in 50 mL of PBS solution in order to simulate body fluid at pH 7.4 and 37 °C.  
123 The samples were stirred at *ca.* 60 rpm and 5 mL aliquots of DDS/PBS were removed at  
124 regular intervals and an equal amount of fresh dissolution medium was added to keep the  
125 volume of mixture constant (50 mL). The aliquots were filtered through a 0.20  $\mu\text{m}$  filter  
126 (Whatman) and analyzed by HPLC. The amount of released 5-FU was calculated using the  
127 equation previously described [36]. Experiments were conducted in triplicate and the values  
128 were averaged. The release studies were carried out for 48 h, corresponding to the time of  
129 contact of DDS with the cells.

#### 130 **2.4. Cell culture conditions and cell viability assays**

131 HCT-15 and RKO were used in this study as models of human colorectal carcinoma. HCT-15  
132 colon carcinoma cells were maintained in RPMI 1640 medium (Gibco) and RKO colon  
133 carcinoma cells were maintained in DMEM medium (Gibco). Both cell lines were  
134 supplemented with 10% (v/v) fetal bovine serum (FBS) (Gibco, Invitrogen, USA) and 1%  
135 (v/v) penicillin-streptomycin solution (P/S) (Invitrogen, USA) and incubated at 37 °C in a 5%  
136 CO<sub>2</sub> humidified atmosphere. Cells were subcultured approximately every three days and  
137 maintained in a log-phase growth.

138 Cell viability was assessed using the *In Vitro* Toxicology Assay Kit, Sulforhodamine B based  
139 (Sigma-Aldrich, St. Louis, MO, USA). HCT-15 (7500 cells/100µL/well) and RKO (6000  
140 cells/100µL/well) cells were seeded in 96-well plates and incubated at 37 °C in a 5% CO<sub>2</sub>  
141 humidified atmosphere for 24 h. In order to assess the effects of the starting zeolites, 5-FU  
142 and DDS used and cells were incubated with increasing concentrations of the systems in  
143 culture medium. Controls were performed with culture medium alone. After an incubation  
144 period of 48 h, the spent media were removed and the plate wells were washed with 1x  
145 Phosphate-buffered solution, pH 7.4 (PBS). After a fixation step with cold 10%  
146 trichloroacetic acid (TCA), cells were stained with 0.4% Sulforhodamine B and the  
147 incorporated dye was solubilized with Sulforhodamine B solubilization solution (10 mM  
148 Tris). Absorbance was monitored with a microplate reader at 570 nm with a background  
149 absorbance of 655 nm. Cell viability was determined as percentage of viability: (OD  
150 experiment/OD control) x 100 (%). Results are presented as mean ± standard deviation (SD)  
151 of three independent experiments, each in triplicate. One-way ANOVA, followed by Dunnett  
152 post test (Fig. 6 and 7) were used to perform cell viability assay statistical analysis. The  
153 previous tests and 50% growth inhibition (IC<sub>50</sub>) were determined using the Graphpad Prism  
154 5<sup>®</sup> software. Values were considered statistically significant in all experiments when  $p < 0.05$ .

#### 155 **2.5. Fluorescence microscopy assays**

156 HCT-15 (10000 cells/500 $\mu$ L/well) and RKO (50000 cells/500 $\mu$ L/well) cell lines were seeded  
157 on coverslips in 24-well plates and incubated at 37 °C in a 5% CO<sub>2</sub> atmosphere for 24 h.  
158 Spent media were removed, cells were washed with PBS 1x and then incubated with 0.025  
159 mg/mL of RhodamineB@NaY during 48 h. Cells were washed twice with PBS-Tween 0.05%  
160 (PBST 0.05%), fixed with cold methanol during 10 min, washed twice with PBST 0.05% and  
161 permeabilized with PBST 0.01% for 10 min.

162 Next, and after two washes with PBST 0.05%, cells were blocked with FBS 10% in PBST  
163 0.05% during 30 min and then incubated with anti- $\beta$ -tubulin antibody (ab6046, Abcam®)  
164 diluted in FBS 5% in PBST 0.05% (1:700) during 1 h at room temperature. In the next step,  
165 cells were washed three times with PBST 0.05% (10 min each) and incubated with the  
166 secondary antibody anti-rabbit Alexa Fluor 488 (A11008, Invitrogen) diluted in FBS 5% in  
167 PBST 0.05% (1:1000) during 1 h at room temperature. Finally, after three washes with PBST  
168 0.05% (10 min each) and one wash with PBS (5 min), cells were mounted in Vectashield  
169 mounting media with 4',6'-diamidino-2'-phenylindole (DAPI) (Vector Laboratories). Images  
170 were acquired in an Olympus IX81 fluorescence microscope (Tokyo, Japan), using Cell P  
171 software.

## 172 **2.6. Characterization methods**

173 The textural characterization of the zeolites was based on the N<sub>2</sub> adsorption isotherms,  
174 determined at -196 °C with a Quantachrome NOVA 4200e apparatus. The samples were  
175 previously outgassed at 150 °C under vacuum. The micropore volumes ( $V_{\text{micro}}$ ) and mesopore  
176 surface areas ( $S_{\text{meso}}$ ) were calculated by the t-method. Surface areas were calculated by  
177 applying the BET equation. Mesoporous size distributions were obtained from the desorption  
178 branch of the isotherm using the Barrett, Joyner and Halenda (BJH) method [37]. Elemental  
179 analyses of carbon, nitrogen, and hydrogen were carried out on a LECO CHNS-932  
180 equipment. Scanning electron micrographs (SEM) were collected on a LEICA Cambridge  
181 S360 Scanning Microscope equipped with an EDX system for NaY and 5-FU@NaY. The

182 morphology of NanoNaY, 5-FU@NanoNaY, LTL and 5-FU@LTL was studied by scanning  
183 electron microscopy using a NanoSEM–FEI Nova 200 (FEG/SEM) equipped with an EDX  
184 system. In order to avoid surface charging, samples were coated with gold in vacuum prior to  
185 analysis, by using a Fisons Instruments SC502 sputter coater.  $^1\text{H}$ - $^{13}\text{C}$  cross-polarization/magic  
186 angle spinning nuclear magnetic resonance ( $^{13}\text{C}$ -CP/MAS NMR) and MAS  $^{27}\text{Al}$  spectra were  
187 recorded on a 9.4 T wide-bore (400 MHz,  $^1\text{H}$  Larmor frequency) Bruker Avance III  
188 spectrometer. A 4 mm double-resonance MAS probe was employed at 100.6 MHz ( $^{13}\text{C}$ ) and  
189 104.2 MHz ( $^{27}\text{Al}$ ) Larmor frequencies. Samples were spun in  $\text{ZrO}_2$  rotors using a spinning  
190 rate of 10 and 14 kHz, respectively for  $^{13}\text{C}$  and  $^{27}\text{Al}$  experiments.  $^{13}\text{C}$ -CP/MAS NMR spectra  
191 were recorded using a ramp step (varying from 100% to 50% in amplitude using 100 points);  
192 contact time: 3.0 ms;  $^1\text{H}$   $90^\circ$  excitation pulse: 2.5  $\mu\text{s}$ ;  $^1\text{H}$  and  $^{13}\text{C}$  radio-frequency field  
193 strengths for CP were set to 87 kHz and 68 kHz, respectively; recycle delay: 5 s. TPPM-15  
194 decoupling was employed during the signal acquisition using a 4.75  $\mu\text{s}$  pulse length for the  
195 basic TPPM pulse unit along the  $^1\text{H}$  channel, employing a  $^1\text{H}$  radio-frequency field strength of  
196 100 kHz.  $^{27}\text{Al}$  spectra were recorded with an excitation pulse length of 0.7  $\mu\text{s}$  (corresponding  
197 to  $10^\circ$  flip angle) and 1 s recycle delay. The release studies were carried out by high  
198 performance liquid chromatography (HPLC – JASCO 980-PU) using an isocratic pump and a  
199 double on line detection including an UV–vis detector and refractometer. A LiChroCart 250-4  
200 RP-18e/5  $\mu\text{m}$  column from Merck with a mobile phase contained a phosphate solution (0.01  
201 M) in methanol/water (60/40) were used for the HPLC assays. The flow rate was 0.4 mL/min  
202 and the injection volume was 20  $\mu\text{L}$  and the absorbance of 5-FU was monitored at 260 nm.  
203 Calibration curve was constructed using solutions of 5-FU with concentrations from 0.0005  
204 mg/mL to 0.10 mg/mL. Room temperature Fourier Transform Infrared (FTIR) spectra of the  
205 samples in KBr pellets were measured using a Bomem MB104 spectrometer in the range  
206 4000-500  $\text{cm}^{-1}$  by averaging 20 scans at a maximum resolution of 4  $\text{cm}^{-1}$ . The loading and the  
207 thermal stability of the samples were determined by thermogravimetric analysis in a STA 409



208 PC/4/H Luxx Netzsch thermal analyser. The atmosphere used was high purity air (99.99 %  
209 minimum purity) with a flow rate of 50 cm<sup>3</sup>/min. The sample holders used were crucibles of  
210 alumina oxide, supplied by Netzsch. The samples were heated between 50 and 700 °C at 10  
211 °C/min to evaluate the thermal stability.

212

### 213 **3. Results and discussion**

#### 214 **3.1. Loading and Physicochemical Characterization of DDS**

215 The method for the preparation of the DDS was the adsorption of 5-FU in liquid phase within  
216 the zeolite pores and channels [30,31] and the resulting DDS were characterized by several  
217 techniques.

218 Loading of 5-FU into the zeolites was determined by thermogravimetric analysis (TGA). All  
219 DDS present the same weight loss in the studied temperature range. Two distinct weight  
220 changes are seen in the TGA data for pure 5-FU around 200-305 °C and 305-410 °C, which  
221 can be attributed to the onset of melting, followed by decomposition of the 5-FU molecule  
222 [38]. In the case of drug-loaded zeolites, the weight change is extended over the entire  
223 temperature range up to 700 °C [39]. A small weight loss at 150 °C was also observed in the  
224 DDS, which can be attributed to the removal of physisorbed water in the zeolite [35,36]. The  
225 TGA curve for the parent zeolites shows the same weight loss around 120 °C. The other  
226 weight changes observed in DDS were similar to the ones of 5-FU.

227 Table 1 shows the 5-FU loading obtained for all prepared DDS. The drug loading studies  
228 revealed significant encapsulation efficiency for NaY followed by nanoNaY and LTL. Both  
229 nanosized zeolites, nanoNaY and LTL, show similar encapsulation efficiency, *ca.* 55 %.

230

231 **Table 1-** Loading of 5-FU in the DDS.

232

DDS	5-FU (mmol) <sup>a</sup>	5-FU (mmol) <sup>b</sup>	Yield (%) <sup>c</sup>
5-FU@NaY	0.99	0.72	71.3
5-FU@nanoNaY	0.99	0.55	55.6
5-FU@LTL	0.99	0.52	52.5

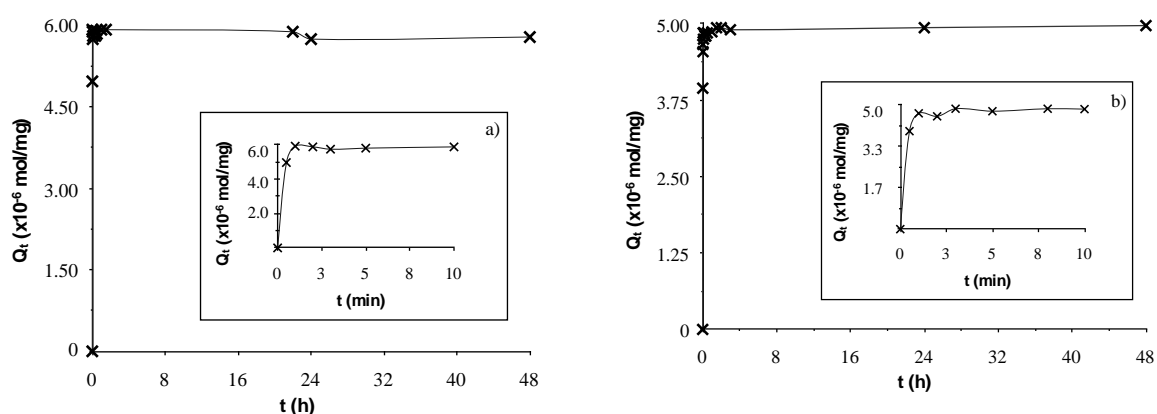
233 <sup>a</sup>Initial 5-FU amount in the solution; <sup>b</sup>5-FU loading in zeolite determined by TGA; <sup>c</sup>Encapsulation  
 234 efficiency of 5-FU in zeolites.

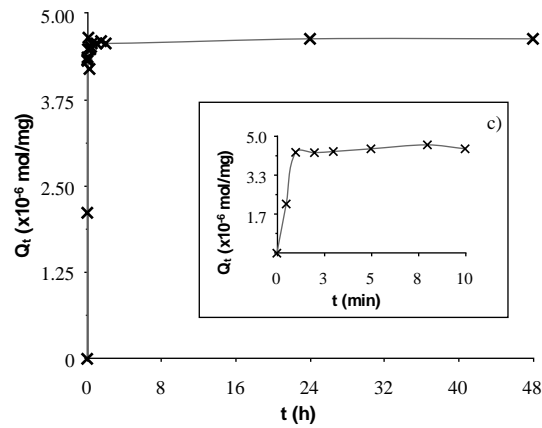
235

236 NaY presents a larger micropore volume than the other zeolites, suggesting that this zeolite  
 237 has a higher capacity for 5-FU loading, since it adsorbs preferentially on the micropores (see  
 238 supplementary data).

239 The release profiles of 5-FU from zeolites, NaY, nanoNaY and LTL are shown in Fig. 1. The  
 240 results were similar, with maxima of 80%, 94% and 89% 5-FU release up to 48 h for NaY,  
 241 nanoNaY and LTL, respectively.

242





243 **Fig. 1.** Release profiles of (a) 5-FU@NaY, (b) 5-FU@nanoNaY and (c) 5-FU@LTL. The  
 244 insets correspond to the 5-FU release from the DDS up to 10 min. The release was  
 245 measured in a phosphate buffer solution (PBS) at pH = 7.4 and 37 °C.  $Q_t = \frac{n_{t_{\text{corr}}}}{W}$ , where  
 246  $n_{t_{\text{corr}}}$  [36] the number of moles at time  $t$  (corrected to account for changes in volume)  
 247 and  $W$  is the weight (mg) of the zeolite.

248

249 All three zeolites show similar initial burst rates of 5-FU release with an exponential-type  
 250 behavior and *ca.* 80-90% 5-FU release in the initial 10 min. The similarity observed in the 5-  
 251 FU release profiles seems to be not dependent of the framework structure of the zeolites, 3D  
 252 (Y zeolite) or 1D (LTL zeolite). The diffusion from within the zeolite pores and channels  
 253 appears to be no different from the internal surface or even from the aggregate of particles.

254 In order to establish the best release profile, the DDS release kinetic profiles were modeled by  
 255 fitting the mathematical kinetic models usually used to describe *in vitro* drug dissolution and  
 256 release from pharmaceutical dosage forms [40], including the zero-order ( $Q_t = Q_0 + K_0t$ ), first-  
 257 order ( $\ln Q_t = \ln Q_0 + K_1t$ ), Higuchi ( $Q_t = K_H\sqrt{t}$ ), Hixson-Crowell ( $Q_0^{1/3} - Q_t^{1/3} = K_s t$ ), Korsmeyer-  
 258 Peppas ( $Q_t/Q_\infty = K_k t^n$ ) and Weibull ( $\log[-\ln(1 - (Q_t/Q_\infty))] = b \log t - \log a$ ) models [40]. The release  
 259 models with major application and best describing drug release are the zero-order, Higuchi,  
 260 Korsmeyer-Peppas and Weibull models [40,41]. The fitted data for the selected release kinetic  
 261 models are listed in Table 2.

262 **Table 2-** Fitted parameters of the kinetic models used in the *in vitro* drug release of DDS.

Mathematical models	5-FU@NaY	5-FU@nanoNaY	5-FU@LTL
<b>Zero order</b>			
$K_0$ ( $h^{-1}$ )	$41.5 \times 10^{-6}$	$1.2 \times 10^{-6}$	$2.5 \times 10^{-6}$
R	0.4416	0.6567	0.5475
<b>Higuchi</b>			
$K_H$ ( $h^{-1/2}$ )	$6.6 \times 10^{-6}$	$1.2 \times 10^{-6}$	$2.6 \times 10^{-6}$
R	0.5943	0.7806	0.6657
<b>Korsmeyer-Peppas</b>			
$K_p$ ( $h^{-n}$ )	1.04	1.06	1.25
$n$	0.03	0.05	0.17
R	0.8361	0.9111	0.8304
<b>Weibull</b>			
$T_i$ (h)	0.002	0.001	0.010
$b$	0.37	0.30	0.51
$a$	0.09	0.13	0.10
R	0.9975	0.9851	0.8988

263  $K_0$ ,  $K_H$  and  $K_p$  are the release rate constants;  $n$  is the release exponent;  $T_i$  is the time parameter (time  
 264 interval necessary to release 50% to 90% of the drug);  $b$  is the shape parameter and  $a$  is the scale  
 265 parameter.

266  
 267 The *in vitro* drug release from zeolites was best described by the Weibull model, as the plots  
 268 showed the highest linearity. The Weibull model is more useful for comparing the release  
 269 profiles of matrix-type drug delivery [41]. This model describes the dissolution curve in terms  
 270 of applicable parameters and is able to empirically describe, but not mechanistically  
 271 characterize, the dissolution behavior of the dosage form. The advantage of the Weibull  
 272 model lies on its ability to fit almost any kind of dissolution curve and it is, therefore, often  
 273 used to describe experimental data, especially when the mechanism of release underlying the  
 274 dissolution behavior is unknown [42]. In this model, the shape parameter,  $b$ , characterizes the

275 curve as exponential ( $b=1$ , case 1), sigmoid, S-shaped, with upward curvature followed by a  
276 turning point ( $b>1$ , case 2), or parabolic, with a higher initial slope and after that consistent  
277 with the exponential ( $b<1$ , case 3) [40-42]. The  $b$  parameter obtained after fitting the release  
278 data was 0.37, 0.30 and 0.51 for 5-FU@NaY, 5-FU@nanoNaY and 5-FU@LTL, respectively.  
279 These values are consistent with case 3 exhibiting higher initial slope followed by an  
280 exponential curvature, as it is evident from the release profiles for all DDS in Fig. 1.

281 The rapid release of 5-FU from zeolites may be rationalized in terms of the size of the drug  
282 and its interactions with the zeolite frameworks. 5-FU is a small molecule with molecular  
283 dimensions  $4.936 \text{ \AA} \times 5.387 \text{ \AA} \times 5.043 \text{ \AA}$ , which can easily diffuse out of the micropores of  
284 faujasite and Linde type L. These zeolite structures have similar pore opening diameters,  
285 which results in the enhanced release of the drug in the buffer solution.

286 The  $^{13}\text{C}$  NMR spectrum of 5-FU shows the characteristic peaks of the drug molecule with  
287 resonances at  $\delta_{13\text{C}} = 161.6$  (C4), 149.5 (C2), 139.3 (C5) and 130.0 (C6) ppm, consistent with  
288 previous assignments [43]. The presence of the 5-FU C2, C5 and C6 peaks in the  $^{13}\text{C}$   
289 CP/MAS spectrum of 5FU@NaY indicates both, the presence and integrity of the drug, and  
290 minimal interactions with the zeolite framework (see supplementary data). The poor signal-to-  
291 noise ratio of this spectrum (despite 22 h of acquisition) does not allow confirmation of the  
292 presence of the C4 resonance, whose observation may also be hindered by longer  $^1\text{H}$   
293 relaxation.  $^{27}\text{Al}$  solid-state MAS NMR spectra of all samples are identical showing that the  
294 experimental procedure used does not damage the structure of the zeolites and providing no  
295 evidence for significant framework-drug interactions.

296 Fourier Transformed Infrared spectroscopy (FTIR) also does not reveal any significant  
297 interactions between the drug and the zeolite (see supplementary data). The 5-FU spectrum  
298 shows the characteristic vibrational modes of the anticancer molecule. The bands at 1722,  
299 1660 and  $1246 \text{ cm}^{-1}$  are attributed to the cyclic imide, CO-NH-CO. The bands at  $1430 \text{ cm}^{-1}$   
300 are attributed to C-H stretching in  $-\text{CF}=\text{CH}-$  and the C-H deformation vibration band in  $-$

301 CF=CH- is observed at  $814\text{ cm}^{-1}$  [4,7,44]. In the region  $2750\text{-}3200\text{ cm}^{-1}$ , the vibrational  
302 stretching modes from C-H and N-H were also observed [7].

303 For the prepared DDS, the FTIR spectra are dominated by the strong bands assigned to the  
304 vibrational modes arising from the zeolite structure. The presence of physisorbed water is  
305 detected by the  $\nu(\text{O-H})$  stretching vibration at  $3410\text{ cm}^{-1}$  and the  $\nu(\text{O-H})$  deformation band at  
306  $1635\text{ cm}^{-1}$ . The bands corresponding to the lattice vibrations are observed in the spectral  
307 region between  $1300$  and  $450\text{ cm}^{-1}$  [25,31]. No shift or broadening in the principal zeolite  
308 vibrational bands occur upon inclusion of the drug, further substantiating that the zeolite  
309 frameworks remain unchanged. The spectra of the DDS display the bands attributed to 5-FU,  
310 with no measurable shifts indicating that the drug is present and not interacting strongly with  
311 the zeolitic frameworks.

312

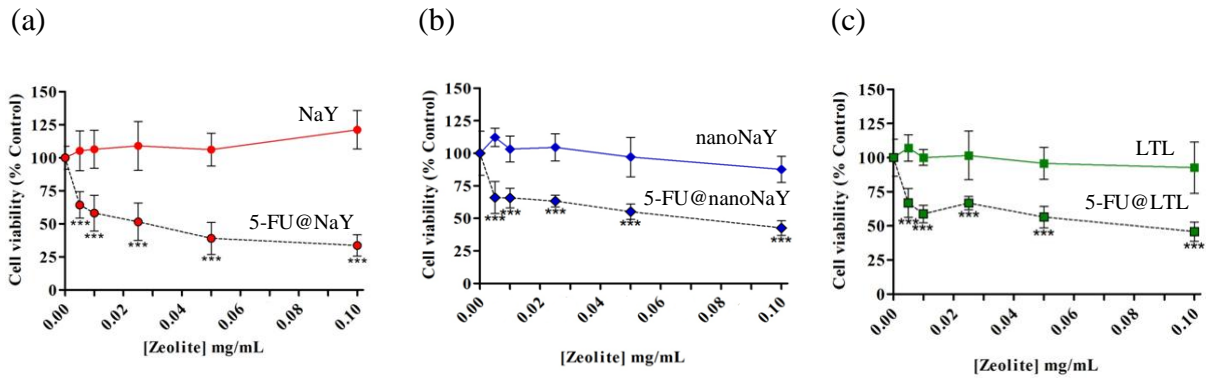
### 313 ***3.2- Drug bioactivity studies***

314 The cytotoxicity studies were carried out in two different cancer cell lines, HCT-15 and RKO.  
315 These lines are well characterized human colorectal carcinoma cells, with different  
316 phenotypes and genetic backgrounds. These cells were chosen as predictive models to test the  
317 potentiation of the chemotherapeutic agent 5-FU into the zeolites NaY, nanoNaY and LTL.  
318 Viability of HCT-15 and RKO cells was evaluated by the sulforhodamine B (SRB) assay,  
319 which measures the drug-induced cytotoxicity and cell proliferation, used for large-scale  
320 drug-screening applications [45].

321 The drug bioactivity studies were performed by preparing five working DDS concentrations,  
322 by diluting a stock suspension ( $1.0\text{ mg/mL}$ ) in culture medium. For better homogenization, all  
323 suspensions were submitted to ultrasonic dispersion for 2 min prior to use. This procedure  
324 was optimized in our previous work [31].

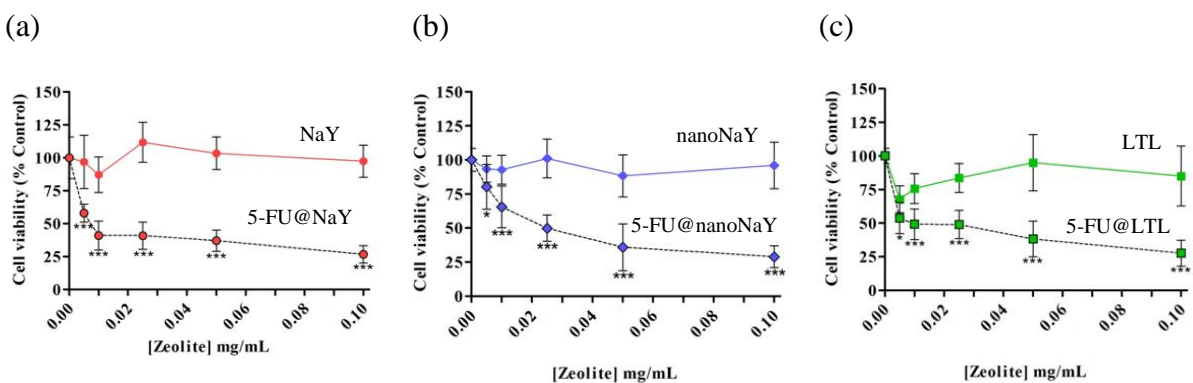
325 The cytotoxicity of the starting zeolites, NaY, nanoNaY and LTL, was investigated in HCT-  
326 15 and RKO cell lines to assess their suitability as DDS. In both cell lines, all zeolites gave

327 similar results according to our previous work, showing no significant toxicity [31]. Fig. 2  
 328 and 3 show the effects on cell viability obtained when treating HCT-15 and RKO cells with  
 329 the non-encapsulated 5-FU and 5-FU@zeolite systems, when taking into consideration the  
 330 amount of drug present in the DDS systems for the different suspensions used.



331 **Fig. 2.** Effect of NaY (a), nanoNaY (b) and LTL (c) zeolites and DDS systems on HCT-15  
 332 colon carcinoma cell viability. HCT-15 cell line was incubated with zeolites and  
 333 different DDS concentrations for 48 h. Cell viability was measured by SRB assay.  
 334 Values are means  $\pm$  SD of three independent experiments, each performed in  
 335 triplicate. \*\*\* $p < 0.001$  compared to zeolite alone.

336



337 **Fig. 3.** Effect of NaY (a), nanoNaY (b) and LTL (c) zeolites and DDS systems on RKO colon  
 338 carcinoma cell viability. RKO cell line was incubated with zeolites and different DDS  
 339 concentrations for 48 h. Cell viability was measured by SRB assay. Values are means

340  $\pm$  SD of three independent experiments, each performed in triplicate. \* $p$ <0.05,  
 341 \*\*\* $p$ <0.001 compared to zeolite alone.

342  
 343 The differences between controls (without zeolite) and the range of zeolite concentrations are  
 344 non-significant, showing in this way that all zeolites are non-toxic to the cells for the selected  
 345 period of incubation and concentrations. Compared to zeolites alone (control), there is an  
 346 evident reduction in cell viability, with increasing concentrations of 5-FU in the zeolite  
 347 system for both cell lines. For HCT-15 cell line, 5-FU encapsulated into NaY, nanoNaY and  
 348 LTL, led to a reduction in cell viability from 64 to 34%, 66 to 43% and 67 to 46% comparing  
 349 with cells treated with the starting zeolite. In RKO cells (Fig. 3), incubation of the 5-  
 350 FU@zeolite systems resulted also in a significant decrease in cell viability for the three  
 351 zeolite systems: from 58 to 27% for 5-FU@NaY, 80 to 29% for 5-FU@nanoNaY and 54 to  
 352 28% for 5-FU encapsulated in LTL zeolite. Moreover, the reduction in viability was more  
 353 pronounced in RKO cell line.

354 5-FU working concentrations (0.01, 0.10, 1 and 10 mM) were obtained by diluting the stock  
 355 solution (1 M) in culture medium. It is possible to observe a dose-dependent decrease in cell  
 356 viability, being the IC<sub>50</sub> values of 0.61 mM for HCT-15 cells and 0.13 mM for RKO (Table  
 357 3).

358 **Table 3-** 5-FU, 5-FU@NaY, 5-FU@nanoNaY and 5-FU@LTL IC<sub>50</sub> values for HCT-15 and  
 359 RKO cell lines.

	HCT-15		RKO	
	IC <sub>50</sub> (mM)	Potentialiation	IC <sub>50</sub> (mM)	Potentialiation
5-FU	0.61	--	0.13	--
5-FU@NaY	0.08	7.6	0.03	4.3
5-FU@nanoNaY	0.21	2.9	0.08	1.6
5-FU@LTL	0.31	1.9	0.03	4.3

360

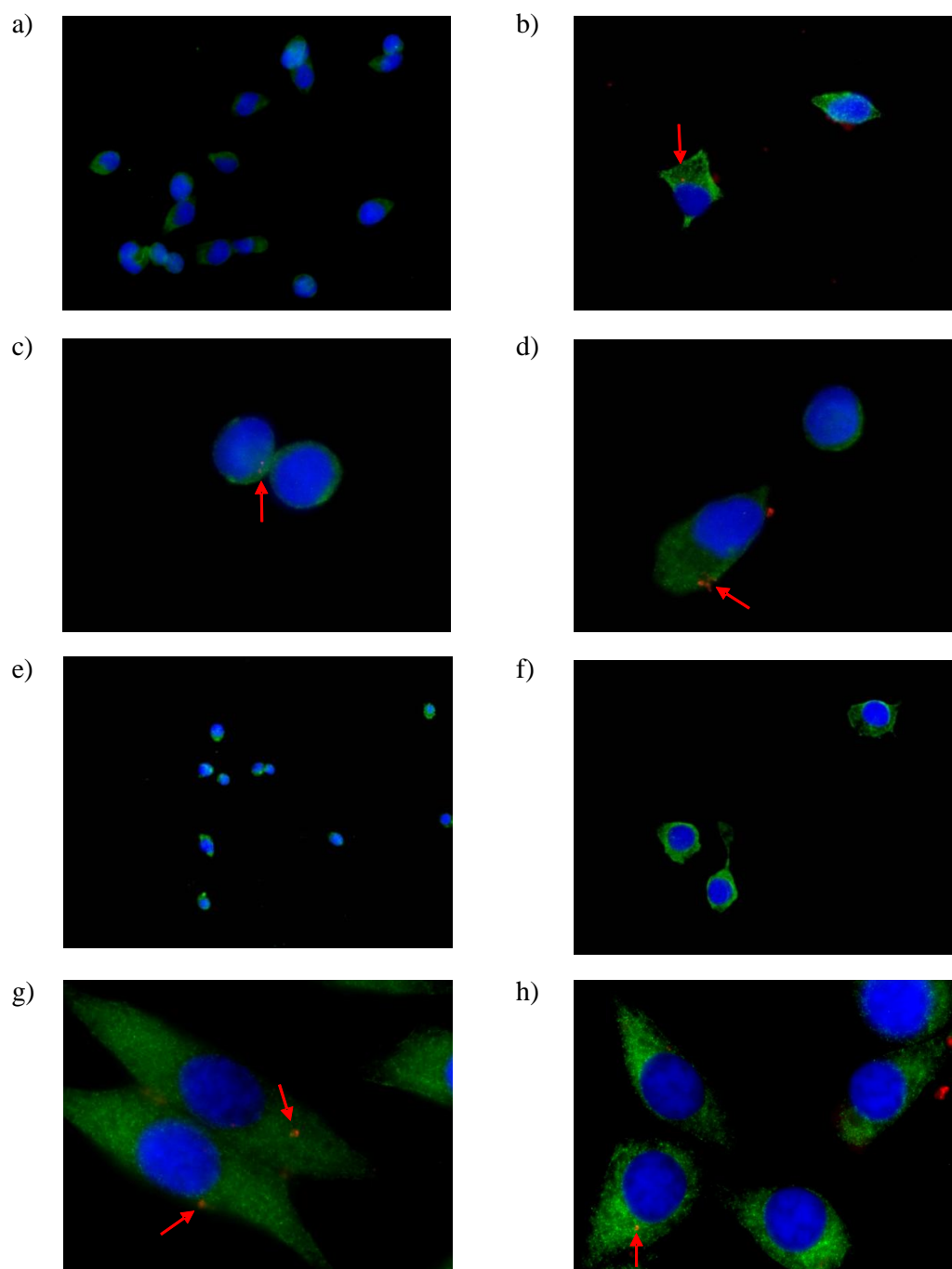


361 By comparing the results obtained when treating cells with the non-encapsulated 5-FU with  
362 the encapsulated 5-FU, there is an obvious potentiation of the effect of the drug. For HCT-15,  
363 there is an increase in efficiency of the drug between 1.9 and 7.6-fold, corresponding to 5-FU  
364 assay concentrations of 0.08 and 0.31 mM, respectively. Likewise, treatment of RKO cells  
365 with the encapsulated 5-FU resulted in a potentiation of the effect of the drug from 1.6 to 4.3  
366 fold.

367 For HCT-15 cells, NaY DDS was more effective than the two remaining nanosized DDS,  
368 probably due to the higher 5-FU loading in zeolite Y. For RKO cells, both NaY and LTL  
369 DDS show the same potentiation. In this case, particle size could have justified the similar  
370 potentiation. However, the different potentiation obtained with LTL in the two cell lines is not  
371 clear, warranting further studies. For higher concentrations of the DDS or starting zeolites  
372 (above 0.25 mg/mL), cell viability began to be affected, likely due to the compromise of cell-  
373 nutrient exchange with the culture media [30,31].

374 In order to assess the interaction between the zeolites and the CRC cells, fluorescence  
375 microscopy assays were performed. Fig. 4 shows the results where HCT-15 and RKO cells  
376 were treated with the NaY zeolite loaded with the fluorescent compound Rhodamine B.

377 Comparing the control images with those with RhodamineB@NaY, it is possible to observe  
378 that the zeolite is able to enter the cell cytoplasm. Although this approach was only applied to  
379 NaY zeolite, it is expected that both nanoNaY and LTL zeolites are also able to enter the cells  
380 due to their smaller dimensions, where internalization would be even easier. Extrapolating  
381 these results for the DDS, it is likely that the drug release is achieved inside the cells if the  
382 DDS is put in contact with them.



383

384

385 **Fig. 4.** Fluorescence microscopy images showing the cellular localization of NaY zeolite  
 386 loaded with Rhodamine B in CRC cell lines (red, arrows). HCT-15 cell line: (a)-(d);  
 387 RKO cell line: (e)-(h); Control: (a), (e) and (f); RB@NaY: (b), (c), (d), (g) and (h).  
 388 Nucleus/DAPI (blue),  $\beta$ -tubulin/FITC (green), RB@NaY/TRITC (red); 200x (e); 400x  
 389 (a) and (f); 600x (b); 1000x (c), (d), (g) and (h).

390

391 By encapsulating 5-FU into zeolites, we increased significantly the efficiency of this drug.  
392 We believe that similarly to other systems [16, 46-48], the zeolite DDS allow the release of 5-  
393 FU, increasing the bioavailability of the drug, and thus explaining the increase in potency.  
394 Moreover, the entry of 5-FU into the cells could also contribute to the high increase in  
395 potency observed. Thus, this potency rise could be the combined result of both the increase in  
396 5-FU bioavailability and the facilitation of 5-FU entry into the cell by the DDS.

397

#### 398 **4- Conclusions**

399 5-FU was successfully loaded into the zeolite structures with different particle sizes, NaY  
400 (700 nm) and two nanosized zeolites, nanoNaY (150 nm) and nanoLTL (80 nm) and the  
401 loading of 5-FU was found to be highest in NaY followed by nanoNaY and LTL. FTIR and  
402 solid-state NMR ( $^{13}\text{C}$  and  $^{27}\text{Al}$ ) provided no evidence for significant framework-drug  
403 interactions. The release of the drug from the zeolite structures in buffer solution at pH = 7.4  
404 and 37 °C followed the Weibull model. The effect of the zeolites and DDS on HCT-15 and  
405 RKO human colon carcinoma cell lines viability was evaluated. DDS based on zeolites were  
406 able to increase the efficiency of 5-FU, a widely used anticancer drug. We believe these  
407 systems should be further explored in other cancer models, e.g. *in vivo* models, to confirm the  
408 efficiency of the systems.

409

#### 410 **Acknowledgments**

411 RA is recipient of fellowship SFRH/B1/51118/2010 from Fundação para a Ciência e a  
412 Tecnologia (FCT, Portugal). This work was supported by the FCT projects refs. PEst-  
413 C/QUI/UI0686/2011 and PEst-C/CTM/LA0011/2011 and the Centre of Chemistry and Life  
414 and Health Sciences Research Institute (University of Minho, Portugal). The NMR

415 spectrometer is part of the National NMR Network (RNRMN), supported with funds from  
416 FCT/QREN (Quadro de Referência Estratégico Nacional).

#### 417 **References**

418 [1] A. Jemal, R. Siegel, E. Ward, Y. Hao, J. Xu, T. Murray, M.J. Thun, *CA Cancer J. Clin.* 58  
419 (2008) 71-96.

420 [2] T. Ishikawa, M. Utoh, N. Sawada, M. Nishida, Y. Fukase, F. Sekigochi, H. Ishitsuka,  
421 *Biochem. Pharmacol.* 55 (1998) 1091-1097.

422 [3] N.J. Meropol, *Eur. J. Cancer* 34 (1998) 1509-1513.

423 [4] F.H. Lin, Y.H. Lee, C.H. Jian, J.-M. Wong, M.-J. Shieh, C.-Y. Wang, *Biomaterials* 23  
424 (2002) 1981-1987.

425 [5] C. Heidelberger, N. K. Chaudhuri, P. Danneberg, D. Mooren, L. Griesbach, R,  
426 Duschinsky, R. J. Schnitzer, E. Plevin, J. Scheiner, *Nature* 179 (1957) 663-666.

427 [6] T. A. Rich, R. C. Shepard, S. T. Mosley, *J. Clin. Oncol.* 22(11) (2004) 2214-32.

428 [7] X. Wang, J. Lin, X. Zhang, Q. Liu, Q. Xu, R.-X. Tan, Z. Guo, *J. Inorg. Biochem.* 94  
429 (2003) 186-192.

430 [8] F. Ciardiello, G. Tortor, *Eur. J. Cancer* 39 (2003) 1348-1354.

431 [9] F. Kabbinavar, J. Schulz, M. McCleod, T. Pattel, J. Hamm, J. R. Hecht, R. Mass, B.  
432 Perrou, B. Nelson, W. F. Novotny, *J. Clin. Oncol.* 23 (2005) 3697-3705.

433 [10] B. J. Giantonio, *Nat. Rev. Clin. Oncol.* 6 (2009) 311-312.

434 [11] D. Odom, B. Barber, L. Bennett, M. Peeters, Z. Y. Zhao, J. Kaye, M. Wolf, J. Wieszorek,  
435 *Int. J. Colorectal Dis.* 26(2) (2011) 173-181.

436 [12] R. F. Ozols, R. S. Herbst, Y. L. Colson, J. Gralow, J. Bonner, W. J. Curran, B. L.  
437 Eisenberg, P. A. Ganz, B. S. Kramer, M. G. Kris, M. Markman, R. Mayer, D. Raghavan,

438 G. H. Reaman, R. Sawaya, R. L. Schilsky, L. M. Schuchter, J. W. Sweetenham, L. T.  
439 Vahdat, R. J. Winn, *J. Clin. Oncol.* 25 (2007) 146-162.

440 [13] C. M. Walko, C. Lindley, *Clin. Ther.* 27(1) (2005) 23-44.

- 441 [14] S. Farquharson, A. Gift, C. Shende, F. Inscore, B. Ordway, C. Farquharson, J. Murren,  
442 Molecules 13 (2008) 2608-2627.
- 443 [15] J.L. Arias, Molecules 13 (2008) 2340-2369.
- 444 [16] Y. Zhu, T. Ikoma, N. Hanagata, S. Kaskel, Small. 6 (2010) 471-478.
- 445 [17] M. Danilczuk, K. Dugopolska, T. Ruman, D. Pogocki, Mini-Rev. Med. Chem. 8 (2008)  
446 1407-1417.
- 447 [18] D. G. Fatouros, D. Douroumis, V. Nikolakis, S. Ntais, A. M. Moschovi, V. Trivedi, B.  
448 Khima, M. Roldo, H. Nazar, P. A. Cox, J. Mater. Chem. 21 (2011) 7789-7794.
- 449 [19] Y.H. Zhang, X.J. Yu, X. . Wang, W. Shan, P.Y. Yang, Y. Tang, Chem. Commun. (2004)  
450 2882-2883.
- 451 [20] A. Corma, V. Fornes, F. Rey, Adv. Mater. 14 (2002) 71-74.
- 452 [21] C. Platas-Iglesias, L. Van der Elst, W.Z. Zhou, R.N. Muller, C.F.G.C. Geraldes, T.  
453 Maschmeyer, J.A. Peters, Chem. A Eur. J. 8 (2002) 5121-5131.
- 454 [22] M. Norek, I.C. Neves, J.A. Peters, Inorg. Chem. 46 (2007) 6190-6196.
- 455 [23] M. Arruebo, R. Fernandez-Pacheco, S. Irusta, J. Arbiol, M. R. Ibarra, J. Santamaria,  
456 Nanotechnol. 17 (2006) 4057-4064.
- 457 [24] M.G. Rimoli, M.R. Rabaioli, D. Melisi, A. Cucio, S. Mondello, R. Mirabelli, E.  
458 Sbignete, J. Biomed. Mater. Res. A. 87A (2008) 156-164.
- 459 [25] M.M. Tsotsalas, K. Kopka, G. Luppi, S. Wagner, M.P. Law, M. Schafers, L. De Cola,  
460 ACS Nano 4 (2010) 342-348.
- 461 [26] N. Ndiege, R. Raidoo, M. K. Schultz, S. Larsen, Langmuir 27 (2011) 2904-2909.
- 462 [27] A. Martucci, L. Pasti, N. Marchetti, A. Cavazzini, F. Dondi, A. Alberti, Micropor.  
463 Mesopor. Mater. 148 (2012) 174-183.
- 464 [28] T. Ceyhan, M. Tatlier, H. Akcakaya, J. Mater. Sci. Mater. Med. 18 (2007) 1557-1562.
- 465 [29] A. Corma, H. Garcia, Eur. J. Inorg. Chem. 6 (2004) 1143-1164.

- 466 [30] N. Vilaca, R. Amorim, O. Martinho, R. M. Reis, F. Baltazar, A. F. Fonseca, I.C. Neves,  
467 J. Mater. Sci. 46 (2011) 7511-7516.
- 468 [31] R. Amorim, N. Vilaca, O. Martinho, R. M. Reis, M. Sardo, J. Rocha, F. Baltazar, A. F.  
469 Fonseca, I.C. Neves, J. Phys. Chem. C. 116 (2012) 25642-25650.
- 470 [32] G. Calzaferri, S. Huber, H. Maas, C. Minkow, Angew. Chem., Int. Ed. 42 (2003) 3732–  
471 3758.
- 472 [33] L. Ferreira, A. M. Fonseca, G. Botelho, C. Almeida-Aguiar, I. C. Neves, Micropor.  
473 Mesopor. Mater. 160 (2012) 126–132.
- 474 [34] I. Kuzniarska-Biernacka, K. Biernacki, A.L. Magalhães, A.M. Fonseca, I.C. Neves, J.  
475 Catal. 278 (2011) 102-110.
- 476 [35] I.C. Neves, C. Cunha, M.R. Pereira, M.F.R. Pereira, A.M. Fonseca, J. Phys. Chem. C  
477 114(24) (2010) 10719-10724.
- 478 [36] A. Datt, D. Fields, S.C. Larsen, J. Phys. Chem. C. 116 (2012) 21382-21390.
- 479 [37] S.J. Gregg, K.S.W. Sing, Adsorption, Surface Area and Porosity, Academic Press, San  
480 Diego, 1982.
- 481 [38] R.J. Lewis, Hawley's Condensed Chemical Dictionary, 14<sup>th</sup> Edition, John Wiley & Sons,  
482 Inc. New York, NY, 2001 (page 507).
- 483 [39] A. Datt, E.A. Burns, N.A. Dhuna, S.C. Larsen, Micropor. Mesopor. Mater. 167 (2013)  
484 182-187.
- 485 [40] P. Costa, J.M.S. Lobo, Eur. J. Pharm. Sci. 13 (2001) 123-133.
- 486 [41] S. Dash, P.N. Murthy, L. Nath, P, Acta Pol. Pharm. - Drug Research 67(3) (2010) 217-  
487 233.
- 488 [42] K. Thelen, K. Coboeken, S. Willmann, J.B. Dressman, J. Lippert, J. Pharm. Sci. 101(3)  
489 (2012) 1267-1280.
- 490 [43] F.G. Vogt, J.A. Vena, M. Chavda, J.S. Clawson, M. Strohmeier, M.E. Barnett, J. Mol.  
491 Struct. 932 (2009) 16–30.

- 492 [44] L. Huang, W. Sui, Y. Wang, Q. Jiao, *Carbohydr. Polym.* 80 (2010) 168–173.
- 493 [45] W. Voigt, Sulforhodamine B Assay and Chemosensitivity, in: *Methods in Molecular*  
494 *Medicine*, vol. 110: Chemosensitivity: Vol. 1: In Vitro Assays, Edited by: R. D.  
495 Blumenthal © Humana Press Inc., Totowa, NJ, 2005 (page 39).
- 496 [46] E. Gultepe, D. Nagesha, S. Sridhar, M. Amiji, *Adv. Drug Delivery Rev.* 62 (2010) 305-  
497 315.
- 498 [47] E. J. Anglin, L. Cheng, W. R. Freeman, M. J. Sailor, *Adv. Drug Delivery Rev.* 60 (2008)  
499 1266-1277.
- 500 [48] J. L. Vivero-Escoto, I. I. Slowing, B. G. Trewyn, V. S. Y. Lin, *Small* 6 (2010) 1952-  
501 1967.
- 502